8-27-2002

A Coupled Land-Atmosphere Simulation Program (CLASP): Calibration and validation

William J. Gutowski Jr.
Iowa State University, gutowski@iastate.edu

Charles J. Vörösmarty
University of New Hampshire

Mark Person
University of Minnesota Twin Cities

Zekai Ötles
Iowa State University

Balázs M. Fekete
University of New Hampshire

See next page for additional authors

A Coupled Land-Atmosphere Simulation Program (CLASP): Calibration and validation

Abstract

We present a model and application designed to study the coupled land-atmosphere hydrologic cycle, following water from its inflow into a region by horizontal atmospheric transport through surface-atmosphere exchange processes and aquifer recharge to outflow as runoff and river discharge. The model includes a two-way water flow among its major reservoirs (atmosphere, vadose zone, groundwater, surface water, river). A unique feature of the model is that phreatophytic interactions are included when the water table intersects the root zone. The model emulates a uniform grid box of an atmospheric general circulation model, but with finer horizontal resolution for the land processes, and forms a test bed for developing continental-scale simulation of the hydrologic cycle. The model is calibrated using the First International Satellite Land Surface Climatology Project (ISLSCP) Field Experiment (FIFE) observations for 1987 and validated using FIFE observations for 1988 and 1989. Four physical factors emerge as important for simulating the FIFE water cycle: effective relative humidity for initiating stable (large scale) condensation, length of the growing season, amount of available soil water, and cloud cover parameterization. Further evaluation uses water table and river discharge measurements for years up to 1993. The model simulates multiyear behavior in the hydrologic cycle reasonably well. Average differences between FIFE observations and simulated fluxes during the calibration period are only a few percent, including fluxes not specifically calibrated. Model-observation differences in surface sensible and latent heat fluxes are larger during the 1988 drought but recover to relatively small values for 1989, suggesting some difficulty in simulating hydrologic extremes occurring outside the calibration conditions. A model sensitivity study using statistical disaggregation to allow precipitation to fall on only a portion of the landscape indicates that spatial disaggregation of precipitation can have strong impact on groundwater storage and surface discharge, potentially improving agreement between observed and simulated streamflow. Water redistributed through the model's aquifer-river network can at times raise the water table high enough for water to seep back to the vegetation root zone and increase evapotranspiration. During relatively dry periods, up to 33% of monthly evapotranspiration was derived from groundwater-supported evapotranspiration, emphasizing the need to quantify better aquifer-atmosphere interaction. The work also demonstrates the feasibility and utility of fully coupled water budgeting schemes.

Keywords

Surface fluxes, Hydrology; FIFE; Surface modeling; Land-atmosphere coupling

Disciplines

Atmospheric Sciences | Climate | Hydrology

Comments

This article is from *Journal of Geophysical Research: Atmospheres* 107 (2002):ACL 3-1, doi:10.1029/2001JD000392. Posted with permission.

Authors

William J. Gutowski Jr., Charles J. Vörösmarty, Mark Person, Zekai Ötles, Balázs M. Fekete, and Jennifer York

A Coupled Land-Atmosphere Simulation Program (CLASP): Calibration and validation

William J. Gutowski Jr.,[1,2] Charles J. Vörösmarty,[3] Mark Person,[4,5] Zekai Ötles,[1,6] Balazs Fekete,[3] and Jennifer York[4]

Received 23 January 2001; revised 26 September 2001; accepted 8 October 2001; published 22 August 2002.

[1] We present a model and application designed to study the coupled land-atmosphere hydrologic cycle, following water from its inflow into a region by horizontal atmospheric transport through surface-atmosphere exchange processes and aquifer recharge to outflow as runoff and river discharge. The model includes a two-way water flow among its major reservoirs (atmosphere, vadose zone, groundwater, surface water, river). A unique feature of the model is that phreatophytic interactions are included when the water table intersects the root zone. The model emulates a uniform grid box of an atmospheric general circulation model, but with finer horizontal resolution for the land processes, and forms a test bed for developing continental-scale simulation of the hydrologic cycle. The model is calibrated using the First International Satellite Land Surface Climatology Project (ISLSCP) Field Experiment (FIFE) observations for 1987 and validated using FIFE observations for 1988 and 1989. Four physical factors emerge as important for simulating the FIFE water cycle: effective relative humidity for initiating stable (large scale) condensation, length of the growing season, amount of available soil water, and cloud cover parameterization. Further evaluation uses water table and river discharge measurements for years up to 1993. The model simulates multiyear behavior in the hydrologic cycle reasonably well. Average differences between FIFE observations and simulated fluxes during the calibration period are only a few percent, including fluxes not specifically calibrated. Model-observation differences in surface sensible and latent heat fluxes are larger during the 1988 drought but recover to relatively small values for 1989, suggesting some difficulty in simulating hydrologic extremes occurring outside the calibration conditions. A model sensitivity study using statistical disaggregation to allow precipitation to fall on only a portion of the landscape indicates that spatial disaggregation of precipitation can have strong impact on groundwater storage and surface discharge, potentially improving agreement between observed and simulated streamflow. Water redistributed through the model's aquifer-river network can at times raise the water table high enough for water to seep back to the vegetation root zone and increase evapotranspiration. During relatively dry periods, up to 33% of monthly evapotranspiration was derived from groundwater-supported evapotranspiration, emphasizing the need to quantify better aquifer-atmosphere interaction. The work also demonstrates the feasibility and utility of fully coupled water budgeting schemes. *INDEX TERMS:* 1655 Global Change: Water cycles (1836); 1836 Hydrology: Hydrologic budget (1655); 3322 Meteorology and Atmospheric Dynamics: Land/atmosphere interactions; 1833 Hydrology: Hydroclimatology; *KEYWORDS:* surface fluxes, hydrology, FIFE, surface modeling, land-atmosphere coupling

1. Introduction

[2] Development of Earth-system models for the study of climate changes requires a comprehensive understanding of the planet's hydrologic cycle. Repercussions of potential climate change may be substantial for hydrologic processes occurring at the land-atmosphere interface, because water plays a central role in many economically important activities such as agriculture and transportation [e.g., *Logaiciga et al.*, 1996]. Typically, the land surface has served as a boundary (often prescribed) for quantitative studies focusing on either the land or the atmospheric branches of the hydrologic cycle. However, there are numerous potential feedbacks between land and atmosphere which require their shared interface to

[1]Department of Geological and Atmospheric Sciences, Iowa State University, Ames, Iowa, USA.
[2]Also at Department of Agronomy, Iowa State University, Ames, Iowa, USA.
[3]Water Systems Analysis Group, Institute for the Study of Earth, Oceans, and Space, and Department of Earth Sciences, University of New Hampshire, Durham, New Hampshire, USA.
[4]Department of Geology and Geophysics, University of Minnesota, Minneapolis, Minnesota, USA.
[5]Now at Department of Geosciences, Indiana University, Bloomington, Indiana, USA.
[6]Now at Frontier Science and Technology Research Foundation, Inc., Madison, Wisconsin, USA.

0148-0227/02/2001JD000392

serve as a gateway between the two domains rather than a boundary. Similarly, the bottom of the vegetation root zone has formed a boundary where water usually flows to aquifers, but often not from aquifers into the root zone and eventually the atmosphere. These couplings create potentially important feedbacks in the water cycle.

[3] To study potential feedbacks between different water reservoirs, we have developed a Coupled Land-Atmosphere Simulation Program (CLASP) that represents hydrologic processes extending from the atmosphere through the land surface to aquifers and, ultimately, river systems. A unique feature of our approach is that it includes two-way, lateral subsurface water transfers among root zones, aquifers, and rivers, thus allowing groundwater-supported evapotranspiration [*Winter*, 2001] when the water table intersects the root zone. In this paper we describe the mathematical formulation of the model and present an initial application with realistic atmospheric forcing. We use this application to calibrate and validate the model using observations for several branches of the land-atmosphere water cycle and related quantities.

[4] Three approaches have been taken in recent years to improve climatic simulation of the terrestrial hydrologic cycle: (1) development of improved land-surface parameterization schemes for direct incorporation into atmospheric general circulation models (AGCMs) [e.g., *Pitman*, 1988; *Dickinson et al.*, 1993; *Sellers et al.*, 1996; *Stieglitz et al.*, 1997; *Koster et al.*, 2000], (2) simulation of regional behavior using atmospheric mesoscale models nested in AGCMs or global data sets to produce output that drives detailed surface hydrologic models [e.g., *Hostetler and Giorgi*, 1993; *Walko et al.*, 2000], and (3) simulation of sub-basin-scale (e.g., 10 km $\times$ 10 km) hydrology in scaling studies that aim at determining how to best represent the effects of spatially varying surface properties in AGCMs [e.g., *Famiglietti and Wood*, 1991; *Salvucci and Entekhabi*, 1995; *Michaud and Shuttleworth*, 1997; *Levine and Salvucci*, 1999]. The first approach has the advantage of allowing a global-scale study of new parameterizations but at relatively coarse (several degrees by several degrees) resolutions. Details of watershed hydrology are neglected in this approach. The last approach offers the finest resolution but does not couple to the scales typically resolved in an AGCM and may not include many, if any, of the feedbacks between surface and atmospheric processes.

[5] This study embraces aspects of each of these approaches. The CLASP emulates a single column of an AGCM but with a spatially distributed representation of land surface processes. Thus as with approach 1, we consider land-atmosphere feedbacks within an AGCM grid box, but as with approach 2, we nest the simulation in a larger-scale atmospheric model, and as with approach 3, we include sub-basin-scale resolution of watershed hydrology. To accomplish this, we implement a data-rich approach advocated earlier [*Vörösmarty et al.*, 1993] which gives the model the ability to incorporate data characterizing its parameters and boundary conditions at spatial resolutions up to the highest available. In this context we use a wide variety of observations to help calibrate and validate model performance. The CLASP emulates the hydrologic dynamics of one atmospheric grid box of a general circulation model. An ultimate motivation for the development of the CLASP is to build a global model of the entire hydrologic cycle that includes water budgets and transports for land, atmosphere, and ocean reservoirs. An important advantage of this approach is that it permits decadal scale simulations of aquifer/atmosphere interactions using conventional computer workstations. The model presented here can be viewed as a first step in the process of constructing a complete, global model of the entire terrestrial hydrologic cycle.

[6] Section 2 of this paper presents a detailed description of the CLASP, broken down into its separate domains, and the coupling between them. In this section we give the fundamental conservation laws governing the CLASP and their ancillary equations. In section 3 we use observations from the First International Land Surface Climatology Project (ISLSCP) Field Experiment (FIFE) [*Sellers et al.*, 1992] to calibrate CLASP. We use additional FIFE observations together with U.S. Geological Survey discharge and water table observations to evaluate further CLASP behavior. Section 4 gives a summary and discussion of the results presented here.

2. Mathematical Model

2.1. Domains and Resolution

[7] The Coupled Land-Atmosphere Simulation Program is a single atmospheric column coupled to an underlying terrestrial domain that may encompass one or more watershed subcatchments. Earlier studies have also used similar one-dimensional (1-D) atmospheric models to study land-atmosphere coupling [e.g., *Wetzel and Chang*, 1988; *Koster and Eagleson*, 1990] and ocean-atmosphere coupling [e.g., *Gutowski et al.*, 1998] in the hydrologic cycle. Because the CLASP emulates a grid box of an AGCM, the atmospheric column's horizontal extent, and hence its horizontal resolution, can range from several tens to hundreds of kilometers, depending on the application. The simulated atmospheric column used here extends from the surface to 19 km. Vertical resolution of the atmosphere ranges from a few tens of meters near the surface to several hundred meters aloft, where less resolution is needed. A higher resolution near the surface is used to resolve the atmosphere's planetary boundary layer (PBL). The terrestrial domain consists of the vegetation, soil, stream channel, riparian zone, and groundwater systems. The terrestrial domain is divided into a number of regularly spaced cells that give the CLASP higher horizontal resolution at the surface than in the atmosphere, allowing us to explore scale-coupling issues. A river network links the cells, with each cell containing one outflow stream. In a typical application the CLASP uses tens to hundreds of terrestrial cells to resolve a watershed at scales down to a few kilometers.

[8] The CLASP consists of three modules (Figure 1): the atmospheric column model (ATMOS), a soil-vegetation-atmosphere transfer (SVAT) model that computes the exchange of water, energy, and momentum between the land surface and the atmosphere, and a groundwater/surface water (GW/SW) model that simulates the flow of surplus water from the SVAT through a subsurface and river drainage network. The modules are designed to be plug compatible [*Kalnay et al.*, 1989]. They also are initial

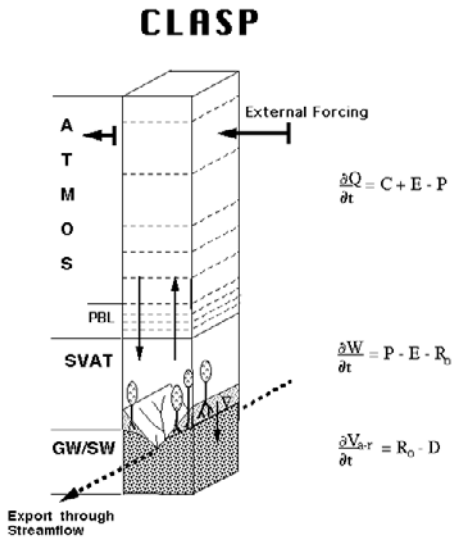

Figure 1. CLASP schematic plus water budget equations. See section 2.5 for an explanation of the budget equations. The vadose zone has fine stipples, while the zone of saturation has coarse stipples.

representations of each domain. The plug compatibility will be exploited to make future stepwise improvements in the model.

[9] To simulate the evolution of the terrestrial water cycle, the CLASP is run for periods of several months to decades. However, many important ATMOS and SVAT processes, such as cumulus convection and evapotranspiration, respond to the diurnal cycle of solar radiation and, in addition, may operate on timescales as small as an hour or less. The usual CLASP time step is thus 15 min. Typical climate AGCMs also use a time step of this order to simulate properly the explicitly resolved atmospheric circulation, so the CLASP temporal discretization is consistent with its intent to emulate an AGCM grid box. Groundwater flow could be simulated reasonably with much larger time steps (days to weeks), but using the same size time step for GW/SW processes incurs a relatively minor computational burden, results in minimal numerical dispersion, and simplifies analyzing the dynamics of the water budget of each module. Time marching is accomplished using a discrete forward step that is computed by implicit finite difference methods, because of the diffusive terms in ATMOS [*Press et al.*, 1992].

2.2. ATMOS

[10] The ATMOS portion of the model has been described in detail elsewhere [*Gutowski et al.*, 1998]; we give a brief description here. Behavior of the atmospheric column is determined by conservation laws for momentum, energy, mass, and water. The governing equations are the flux-form hydrostatic primitive equations [e.g., *Lorenz*, 1967], with an added equation for water vapor conservation. This is essentially the same set used by AGCMs but in a single column only. Temporal changes of prognostic variables due to horizontal convergences are specified from a three-dimensional analysis of the atmosphere using an upstream method based on the *Randall and Cripe* [1999] relaxation scheme. Analysis fields, used to force the CLASP, are usually available at most only every 6 or 12 hours. The model determines fields at intermediate times by linear interpolation in time. As an AGCM, the model also includes parameterizations for boundary layer processes [*Louis*, 1979; *Louis et al.*, 1981], atmospheric radiative transfer [*Liou and Ou*, 1981, 1983; *Liou and Zheng*, 1984], cumulus convection [*Emanuel*, 1991], and stable precipitation. Parameterizations used to compute exchanges of moisture, heat, and momentum with the surface are discussed in the SVAT description.

[11] The model does not explicitly include a condensed-water conservation equation since the mass of water in the condensed phase is usually only a small portion of the total water mass in the atmosphere. When condensed water does form, through supersaturation or cumulus convection, it immediately either falls from the atmosphere as precipitation or reevaporates as it drops through drier air. In this initial version of the CLASP, precipitation is distributed evenly over the surface. Cloud cover is diagnosed for the purposes of radiative-transfer computations, using the parameterization of *Slingo* [1987], but since there is no condensed water budget equation, the mass of cloud water is not part of the water budget computations. This approach for handling condensed water occurs in many AGCMs, though it is not universal [cf. *Phillips*, 1995].

2.3. SVAT

[12] The CLASP SVAT simulates the behavior of the soil zone actively engaged in moisture, heat, and momentum exchanges with the atmosphere and in supplying water to aquifers and, ultimately, open channels. In this version of the CLASP the exchange zone is represented by a layer extending from the surface to the rooting depth of active vegetation, topped by a canopy layer. Any moisture draining from the root zone is assumed to recharge the underlying aquifer. This initial structure is relatively simple to facilitate understanding the coupling between the three CLASP modules (Figure 1). For each cell, we specify vegetation type, soil type and texture, surface roughness, and surface albedo. Because these characteristics can vary from cell to cell across the surface of the computational domain, the SVAT presents a potentially complex mosaic of surface exchanges with ATMOS. The impact of such surface spatial complexity within a single atmospheric column is one direction of future study.

[13] Soil moisture W in each SVAT cell is increased by precipitation (P) and depleted by evapotranspiration (E) and may be increased or decreased by groundwater exchange (R_o) with subterranean aquifers:

$$\frac{dW}{dt} = P - E - R_o. \tag{1}$$

When soil moisture exceeds the holding capacity of the active layer (i.e., root zone), surplus water is treated as groundwater recharge to the underlying aquifer. The root zone may also receive water from the aquifer if the aquifer rises sufficiently to encroach into the root zone.

[14] The SVAT calculates evapotranspiration using the Penman-Monteith scheme [e.g., *Dingman*, 1994], which was found to have relatively low bias when tested in several

hundred well-gauged watersheds across the United States [*Vörösmarty et al.*, 1998]. Thus

$$E = \frac{\frac{de_s(T_a)}{dT}\{R_{\text{net}} + H_{\text{deep}}\} - \rho c_p C_{at}\{e_s(T_a) - e_a\}}{\frac{de_s(T_a)}{dT} + \gamma\left(1 + \frac{C_{at}}{C_{can}}\right)}, \quad (2)$$

where e_s is the saturation vapor pressure, T_a and e_a are the temperature and vapor pressure, respectively, of the atmospheric layer adjacent to the ground, R_{net} is the net surface radiation, and H_{deep} is a heat flux into the ground described in detail below. Other symbols are defined in the Notation section. The atmospheric conductance C_{at} is computed from

$$C_{at} = k^2|\vec{V}_a|\{\ln(z_a/z_o)\}^{-2}, \quad (3)$$

where k is the von Karman constant, $\vec{V}_a$ is the horizontal wind in the atmospheric layer adjacent to the ground, z_a is the midlevel of this layer, and z_o is surface roughness. The canopy conductance C_{can} is given by

$$C_{\text{can}} = c_{\max}\text{LAI}(G_{\text{LWP}}G_{\text{LEAF}}G_{\text{SOL}}G_{\text{HD}}), \quad (4)$$

where $c_{\max}$ is a maximum leaf conductance, and LAI is the leaf-area index. The G terms are conductance multipliers, each ranging between 0 and 1 and each dependent on a physical property. The leaf-water potential coefficient G_{LWP} varies with available soil moisture; the leaf-temperature coefficient G_{LEAF} varies with near-surface air temperature; the solar flux coefficient G_{SOL} varies with net solar (shortwave) radiation; and the absolute humidity deficit coefficient G_{HD} varies with the difference between saturation and actual atmospheric humidity. The functional forms for each G used here follow prescriptions in the work of *Dingman* [1994] with parameters in G_{LWP} adjusted in part using specifications of *Running and Coughlan* [1988] and parameters in G_{HD} adjusted on the basis of field-study results reported by *Stewart and Verma* [1992]. The coefficient G_{LEAF} is further adjusted as part of the model's calibration. The net effect of the conductance coefficients is to produce a feedback between E and soil-water status.

[15] The SVAT includes a canopy that intercepts precipitation, reevaporates it, and spills water to the surface. In the formulation used here, the canopy intercepts all precipitation, filling a canopy reservoir distinct from the soil-moisture reservoir. Water fills this reservoir to its limit before it can overflow and spill to the ground. Water evaporates from the canopy using (2) without H_{deep} and with zero canopy resistance. No evapotranspiration through vegetation occurs while there is water in the canopy reservoir. The depth of the canopy reservoir is proportional to LAI and is determined as part of the calibration.

[16] The sensible heat flux H and the momentum exchange $\vec{M}$ between the surface and the atmosphere are computed using drag laws,

$$H = \rho C_p C_{dh}|\vec{V}_a|(T_s - T_a), \quad (5)$$

$$\vec{M} = \rho C_{dm}|\vec{V}_a|\vec{V}_a, \quad (6)$$

where T_s is the surface temperature. The drag coefficients C_{dh} and C_{dm} are computed as part of the *Louis* [1979] and *Louis et al.* [1981] PBL turbulent dynamics and so are dependent on the temperature structure of the PBL and the surface roughness parameter. For numerical stability in ATMOS, we compute H using a predictor-corrector scheme.

[17] The SVAT advances the surface temperature in time using

$$C_s\frac{\partial T_s}{\partial t} = R_{\text{net}} - H - LE - H_{\text{deep}}, \quad (7)$$

where H_{deep} is a deep-ground heat flux computed using a force-restore method [*Deardorff*, 1978]. Associated with the force-restore method is a deep-ground temperature T_{deep} that evolves in time according to

$$C_{\text{deep}}\frac{\partial T_{\text{deep}}}{\partial t} = H_{\text{deep}}. \quad (8)$$

Variables and parameters in (7) and (8) are defined in Notation. The soil heat capacity, density, and thermal diffusivity vary with soil moisture, with details depending on the soil texture of the specific application.

[18] Finally, although the applications of CLASP later in this paper are for a region with generally small amounts of transient snow, the SVAT also includes the snow model of *Dickinson et al.* [1993] to accumulate and melt snow. So long as snow is falling or present on the surface, its reservoir has priority over the canopy and ground for exchanging water with the atmosphere, through precipitation and sublimation.

2.4. GW/SW

[19] Groundwater flow within each terrestrial grid cell accounts for net recharge from the SVAT, time-dependent subsurface flow down hydraulic gradients, and water exchange between the aquifer and the river network. All water flows are potentially bidirectional. The governing transmissivity-based equation for groundwater flow used in the GW/SW module is [*Konikow and Bredehoeft*, 1974]

$$S_y\frac{\partial}{\partial t}h = \vec{\nabla}\cdot\left(T_h^f\vec{\nabla}h\right) + R_o, \quad (9)$$

where h is water table elevation, and other variables used in (9) are defined in Notation. The transmissivity T_h^f is the product of saturated thickness and aquifer hydraulic conductivity. Recharge across each cell is assumed to be constant over a given time step. Aquifer properties are permitted to vary from cell to cell depending on the model domain's geology. Equation (9) is intended to represent shallow groundwater flow within a phreatic aquifer that is in good hydrologic connection to a river. While this formulation of subsurface water dynamics is idealized, it is able to account for spatial variability of aquifer hydraulic properties as well as capture the gross features of water table response to changing recharge conditions. These processes cannot be represented easily by simpler lumped-parameter formulations of aquifer hydrodynamics [*Gelhar and Wilson*, 1974].

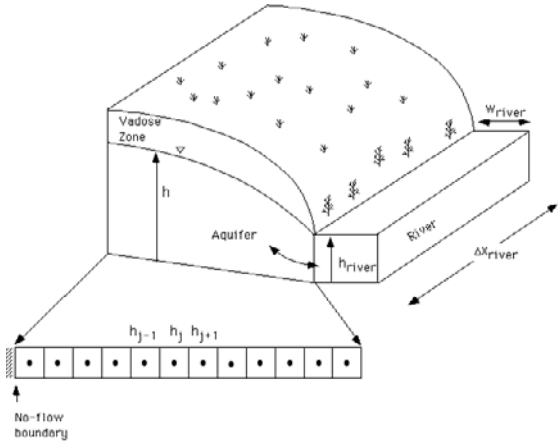

Figure 2. Schematic illustrating different components of the groundwater/surface water domain and the numerical grid used to simulate groundwater flow.

[20] Equation (9) is solved for each SVAT cell using a one-dimensional array (Figure 2) together with a no-flux boundary condition at the cell's upland edge and a base flow $Q_{b\text{-}f}$ from the aquifer to the river given by the Darcy law,

$$Q_{b-f} = -2T_h^f \vec{\nabla} h\Big|_{\text{river}} \Delta X_{\text{river}}, \tag{10}$$

where $\vec{\nabla} h|_{\text{river}}$ is the hydraulic gradient from the aquifer to the river interface, and ΔX_{river} is the length of a cell's side. The factor of 2 in (10) occurs because the stream is assumed to be in the center of each cell; groundwater/stream interactions occur symmetrically on both sides of the river. Thus only local (within cell) groundwater flow is possible. Equation (10) uses the simplifying assumption that the river channel extends down to the base of the aquifer.

[21] In headwater cells, most of the flow is toward the river. However, in low-lying reaches, flow from the river into the aquifer can occur if hydraulic gradients reverse, as when streamflow generated upstream passes through lower reach channels possessing a small topographic gradient. If sufficient flow into the aquifer occurs, the top of the aquifer (water table) can encroach into the vegetation's root zone. When this occurs, encroached nodes have water for evapotranspiration extracted directly from the aquifer, with the leaf-water stress coefficient G_{LWP} set to its no-stress value 1. The water table potentially can rise so high that it floods the surface. In this case, computation of river volume to determine downstream water flow includes the floodwater.

[22] River flow is simulated by a set of differential equations representing each discretized river reach. Within each river element,

$$\frac{\partial V_{\text{river}}}{\partial t} = D_u - D_d + Q_{b-f}, \tag{11}$$

where V_{river} is the volume of water in the river reach, D_u is the sum of all upstream discharge inputs, and D_d is discharge outflow. Although D_d defines the downstream flux of water from a particular cell, it also serves as an upstream input in the continuity equation for its adjacent downstream reach. Channel flow through a cell is represented by Manning's equation

$$D_d = \frac{A_r}{n_m} R_{\text{hyd}}^{2/3} S^{1/2}, \tag{12}$$

where n_m is Manning's roughness coefficient, A_r is the cross-sectional area of the river, R_{hyd} is the hydraulic radius, and S is the slope of the energy grade line [*Streeter and Wylie*, 1979]. River bed geometry can be specified from field survey or inferred from geomorphologic principles in different climatic and topographic zones. At each time step, we assume a uniform river height within an element. In using Manning's equation, we assume steady state discharge over a model time step, and in the model, we further assume that the streambed elevation may be used to calculate the slope S.

2.5. Water Budget Analysis Equations

[23] Part of our analysis of model behavior focuses on water budgets simulated in CLASP. Guided by *Roads et al.* [1994] and references therein, Figure 1 shows the budget equations used for each of the physical domains: ATMOS, SVAT, and GW/SW. The equations are spatially averaged over the CLASP drainage basin.

[24] For ATMOS,

$$\mathrm{Q} = \int_0^\infty \rho q \, dz \tag{13}$$

is the amount of atmospheric water vapor in the column. Also in the atmospheric budget,

$$\mathrm{C} = -\nabla \cdot \int_0^\infty \rho q \vec{\nabla} \, dz \tag{14}$$

is the horizontal convergence of atmospheric water vapor into the column. We compute terms for the model's atmospheric water budget by summing over all atmospheric layers. Consistent with discussion in the previous section, condensed atmospheric water is not included in the budget except when it falls out as precipitation. Also in Figure 1, V_{a-r} is the total water volume in the combined aquifer-river system divided by the basin's area, and D is the net discharge from the basin, again divided by its area.

3. Calibration and Validation

3.1. Observations

[25] We use the set of FIFE observational data from the Konza Prairie Research Natural Area (KPRNA) that was prepared by *Betts and Ball* [1998] for both calibration (1987 observations) and validation (1988 and 1989 observations). We also use U.S. Geological Survey observations of river discharge [*USGS*, 2000] and water table elevations [*Putnam et al.*, 1997] for further assessment of model behavior.

[26] *Duan et al.* [1996] conclude that FIFE observations in 1987 give a good depiction of the area's hydrologic

Table 1. SVAT Grassland Parameters

Parameter	Value
Leaf area index	1.5
Surface roughness, m	0.04
Surface albedo	0.20

cycle. *Betts and Ball* [1998] express some caution, especially for 1988, when the observations do not close the area's water budget very well. Although there is some forest in the region at lower elevations along rivers, the observations occur in grassland. In the *Betts and Ball* [1998] data set, all available FIFE observations of a field such as surface latent heat flux are averaged together at 30-min intervals. The averaging makes no distinction between instruments, nor does it use any differential weighting such as area weighting.

[27] *Betts and Ball* [1998] also give the standard deviation of the reported values at each time step as well as the number of instruments contributing to the average. For most days used, there are typically several instruments reporting values. There are a number of reasons for the range of values among the measurements. These include spatially varying cloud cover [*Smith et al.*, 1992] and physical features of the landscape, such as a site's terrain-slope orientation [*Nie et al.*, 1992a] and specific vegetation characteristics (burned/unburned and grazed/ungrazed grassland) [*Smith et al.*, 1992]. Instrumentation differences also contribute to the disparity. For example, surface latent heat flux measurements were made by both eddy-correlation and Bowen ratio instruments, giving slightly different results [*Nie et al.*, 1992b]. Finally, differences are also caused by measurement error [*Kanemasu et al.*, 1992].

[28] We have used the standard deviation among concurrent measurements to give a metric for how accurately surface fluxes have been simulated. This spread occurs partly due to physical differences between each FIFE observing site and so indicates limits to how precisely one could calibrate the model. Thus our plots of FIFE observations versus time typically show two curves, the instrument average plus/minus the standard deviation. We almost always apply a multiday running average to flux figures to remove daily fluctuations and highlight climatological behavior. In this instance we also apply the running average to the variance among concurrent measurements. Running averages typically use 31-day windows to highlight climatological behavior, which is the focus of our effort, but we resort to a 5-day window, identified when used, when data gaps prevent computation of meaningful time series.

[29] The primary calibration targets from the FIFE data set are time series of elements of the hydrologic cycle: surface latent heat flux, precipitation, and cloud cover. Several other fields not specifically targeted for calibration were also included in model-observation comparisons: surface sensible heat flux, near-surface temperature, heat flux into the ground, surface radiation, runoff, and water table levels.

3.2. Initial and Boundary Conditions

[30] Consistent with our FIFE reference observations, we assume that CLASP is simulating a pure grassland in the central United States at (39°N, 96.5°W) with leaf-area index, surface roughness, and surface albedo given in Table 1. The simulation domain is an 80 km × 80 km region surrounding the FIFE site that uses 2 km × 2 km cells to resolve the observed surface topography and river network (Figure 3). For the simulations here, aquifer conductivity is 10^{-5} m s^{-1} except in fluvial zones adjacent to river segments, where it is 10^{-3} m s^{-1}. The lower value is consistent with a limestone aquifer, while the higher value is consistent with sand and gravel fluvial deposits. Simulated groundwater and discharge are sensitive to these choices. Early model tests using somewhat lower conductivities gave an unrealistic (for this area) concentration in the domain's uplands of high water tables that were intersecting the surface. River segment width and the portion of a cell that is fluvial is a function of surface elevation, corresponding roughly to features of the FIFE and surrounding regions (Table 2). The Kansas River provides the domain with river inflow, which we ignore here to concentrate on the discharge generated within the simulation domain and its coupling with the domain's water cycle.

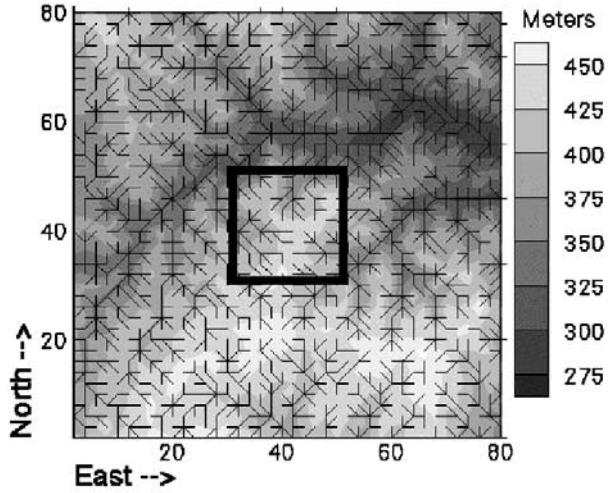

Figure 3. Model topography and river network. The FIFE region is in the box. Axis units are kilometers.

[31] The soil is assumed to be a form of silty-clayey loam [*National Soil Survey Center* (*NSSC*), 2000; *Famiglietti et al.*, 1992]. On this basis we specify soil density, heat capacity, and thermal diffusivity as functions of soil moisture (Table 3) by averaging values given by *Garratt* [1992] for clay and sand. We use linear interpolation to specify these properties at soil moistures intermediate to those given in Table 3.

Table 2. Elevation-Dependent Aquifer/River Properties

Surface Elevation, z_s, m	River Width, m	Fluvial Zone[a], %
$z_s < 300$	30	100
$300 < z_s < 350$	10	20
$350 < z_s$	2	0

[a] Fluvial zone aquifer conductivity is equal to 10^{-3} m s^{-1}; nonfluvial zone aquifer conductivity is equal to 10^{-5} m s^{-1}.

Table 3. Soil Properties Versus Fractional Available Soil Moisture

Available Soil Moisture, %	Density, kg m^{-3}	Heat Capacity, J kg^{-1} K^{-1}	Thermal Diffusivity, m^2 s^{-1}
0	845	1600	0.205×10^{-6}
50	1215	1800	0.68×10^{-6}
100	1515	2000	0.63×10^{-6}

[32] The bedrock aquifer within the model's study domain is characterized by Permian age alternating layers of limestone (1–2 m) and shale (2–10 m) [*Smith*, 1990], with some Pennsylvanian age sandstone-limestone units. The Permian aquifer is overlain by Pleistocene glacial drift and fluvial deposits. Below this aquifer system is a deeper Paleozoic aquifer, which is recharged in Colorado near the Rocky Mountain Thrust Belt. Throughout most of Kansas, there is a modest vertical upflow of groundwater out of the Paleozoic aquifer into the overlying deposits. Flow rates within the Paleozoic aquifer are several orders of magnitude smaller than rates in the shallower aquifer systems, so this deep source of groundwater is not represented in our model. *Macpherson* [1996] suggests that some of the Permian limestone in the Konza Prairie Research Natural Area may be solution enlarged. Slug tests have indicated that the hydraulic conductivity in the KPRNA limestone and shale layers ranges from 10^{-8} to 10^{-3} m s^{-1} [*Macpherson*, 1996]. *Macpherson*'s [1996] study of the KPRNA hydrogeology shows annual variability of water levels in alluvium and limestone wells of 1–2 m. Yearly ground and surface water withdrawals for rural domestic, livestock, municipal, irrigation, and industrial use totals at most 3% of yearly streamflow.

[33] Atmospheric forcing for these simulations is prescribed using output from the operational forecast and data assimilation system for the nested grid model (NGM) of the U.S. National Centers for Environmental Prediction (NCEP). The NGM analyses give temperature, wind, and moisture fields every 50 mbar (5×10^3 Pa) in the lower atmosphere, which is relatively high resolution compared to some other readily available operational analyses of the atmosphere. Since we are focusing on the hydrologic cycle, higher resolution near the surface, where absolute amounts of water vapor are largest, is desirable. We use analysis output from the four NGM grid points surrounding this location to compute the horizontal boundary conditions for the model. The NGM grid points are ~150 km apart, with the CLASP domain approximately in the center of the box they outline.

[34] The NGM analysis gives the state of the atmosphere at 0000, 0600, 1200, and 1800 UTC. Although there are few upper air observations available at 0600 and 1800 UTC, we have found that using the analyses for these times is important for the water balance because the 0600 UTC analysis includes the nocturnal low-level jet, a strong airflow from the Gulf of Mexico into the central United States, which is important for the region's hydrologic cycle [*Stensrud*, 1996].

[35] We have also found that the atmospheric relative humidity in the NGM analyses for this region tends to be low when compared to atmospheric soundings at nearby sites (Figure 4). This deficiency appears to be fairly constant throughout the year, with the observations, on average, having 12% larger specific humidity. As a consequence, for the simulations here, we have increased NGM atmospheric humidity by 12% on input, subject to the restriction that input relative humidity does not exceed 100%.

3.3. Calibration

[36] For the calibration simulations, we use NGM analyses from a 3-year period, 1 January 1985 to 31 December 1987, to drive the CLASP. To arrive at appropriate initial conditions, we cycle through these 3 years repeatedly until soil moisture changes by less than 1% from the start of one 3-year cycle to the next and the aquifer water amount changes by less than 2%. To simplify this stage of the computation, we allow water to spill from the soil to the aquifer but do not permit any aquifer encroachment into the root zone. This assumption appears reasonable for the FIFE observations, which have very few valley bottom sites [*Smith et al.*, 1992] and are not likely to receive significant soil moisture replenishment from aquifer encroachment into the root zone.

[37] The years 1985–1987 do not show any extreme climatic behavior in atmospheric driving data, so we assume that the state to which the model evolves during spin-up is a representative initial condition. Prior to spin-up, initial coarse calibration was performed through a sequence of 80-day sensitivity simulations spanning 1 July to 8 September 1987. The model was then spun-up to create an initial state assumed to apply to 1 January 1985. Final calibration was performed by running the model from 1 January 1985 to 31 December 1987, using the spun-up state as initial condition for soil and atmospheric water.

[38] Four aspects of model construction emerged as important calibration factors for simulating FIFE precipitation, evapotranspiration, and cloud cover: effective relative humidity to initiate stable (large scale) condensation, length of the growing season, amount of available soil water, and cloud cover parameterization. We also calibrated the depth of the canopy reservoir during this phase. Final calibration was based on visual comparison of the temporal evolution of observed and simulated variables and error statistics. One could perhaps increase the precision with which adjusted parameters were chosen by minimizing objective error

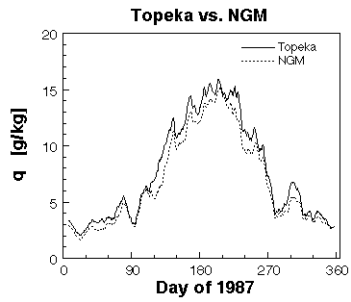

Figure 4. Specific humidity (q) at 950 hPa during 1987 from NGM analyses (39.5°N, 95.2°W) and nearby observations at Topeka, Kansas (39.1°N, 95.6°W). Data have been subjected to a 31-day running average.

Table 4. Original and Adopted Values of Adjusted Parameters

Parameter	Original	Adjusted
RH_{eff}, %	100	93.5
CP, %	15	2.5
RD, m	1.25	1.42
AWC, m	0.162	0.241
T_{oo}, K	273	278
Canopy reservoir depth, m	0.0	$10^{-4} \times$ LAI

functions, but the expository physics of the model would not have been improved in any significant way.

3.3.1. Precipitation

[39] To initiate condensation, the model's original treatment allowed water condensation when relative humidity exceeded 100% at the end of a time step (Table 4). This resulted in deficient precipitation. Operational weather prediction models have sometimes used a simple assumption that the effective saturation relative humidity RH_{eff} is less than 100% [e.g., *Sela*, 1980]. We adopted this assumption for calibrating CLASP precipitation, which was more sensitive to variations of RH_{eff} than to any other adjustment of model parameters. The reasoning behind the assumption is that spatial variability in humidity may cause parts of a layer in a grid box to become saturated even when grid-box-average relative humidity is less than 100%. However, using $RH_{eff} <$ 100% essentially is a correction for bias in the model. The relatively coarse grid of the driving analysis (165 km $\times$ 165 km) compared to the FIFE domain ($\sim$15 km $\times$ 15 km) may be one source of bias because atmospheric moisture convergence will be smoothed somewhat on the coarser grid, resulting in less intense moisture convergence. In addition, atmospheric mass convergence will be less intense, resulting in weaker vertical motion and thus less vertical moisture advection.

[40] Some additional adjustment was made to the convection scheme, where the fraction of precipitation falling outside the convective cloud, *CP*, may be adjusted (K. A. Emanuel, private communication, 1995). The parameter *CP* was reduced to one sixth its original value. This also yielded a small increase in precipitation. In addition, this adjustment retained an approximately even split between stratiform and convective precipitation. Although real-world precipitation is obviously much more complex than a simple split between two types of precipitation, this partitioning is similar to typical behavior of mesoscale models over the United States [e.g., *Pan et al.*, 1999]. We mutually adjusted RH_{eff} and *CP*, so simulated precipitation during the 1987 FIFE observing period nearly matched the observed cumulative precipitation (Table 5), while retaining the approximately even split between stratiform and convective precipitation. Adopted values for RH_{eff} and CP appear in Table 4.

3.3.2. Cloud cover

[41] The primary adjustment of the cloud cover parameterization changed the dependence of stratiform cloud cover on relative humidity, making it consistent with the onset of stratiform precipitation. Thus stratiform cloud cover is 100% when relative humidity equals RH_{eff}.

3.3.3. Available soil moisture

[42] The model's original prescription for grassland rooting depth (RD) was 1.25 m, with the maximum available water capacity (AWC) equal to 13% of RD, or 0.162 m. For the period 28 May to 15 October 1987, when both evapotranspiration E and precipitation P measurements were made, the amount of water lost from the soil was at least $(E - P) = 0.185$ m, so the original water capacity of the soil was too small versus observations. We adjusted both the rooting depth and the maximum available water capacity to help give adequate water-holding capacity to the soil and to obtain surface latent heat flux similar to the FIFE average for 1987 (Table 5). When precipitation amounts were calibrated, E was more sensitive to RD and available water fraction than to other parameters. Adjusting RD and available water fraction had little effect on time-average precipitation, so E could be calibrated somewhat independently of P. Final values of RD and AWC appear in Table 4.

3.3.4. Effective growing season

[43] One of the conductance coefficients in (4), G_{LEAF}, depends on the near-surface air temperature:

$$G_{\mathrm{LEAF}} = \begin{cases} 0 & T_a \le T_{oo} \\ \dfrac{(T_a - T_{oo})\left\{(40 + T_{oo} - T_a)^{1.18}\right\}}{691} & T_{oo} < T_a < (40 + T_{oo}), \\ 0 & (40 + T_{oo}) \le T_a \end{cases} \tag{15}$$

where temperatures are in Kelvin and originally $T_{oo} = 273$ K. We have used this function to control green-up and senescence in the model, in essence making them tem-

Table 5. CLASP Versus FIFE for 1987 Calibration Period[a]

	Comparison Period (Julian Days)	Observation Mean	CLASP-FIFE Mean	Observation Standard Deviation	CLASP-FIFE Standard Deviation
Latent heat, W m^{-2}	162–274	113	+ 3	22	5
Precipitation, mm d^{-1}	121–364	2.5	− 0.04	8.2	7.7
Cloud cover, %	149–235	30	− 0.3	18	10
	260–287				
Sensible heat, W m^{-2}	162–274	25	− 1	9	6
Incident solar, W m^{-2}	136–349	210	+ 4	83	21
Downward infrared, W m^{-2}	157–349	340	+ 3	48	9
Heat flux into soil, W m^{-2}	172–274	− 5	+ 6	6	7

[a] All fluxes were subjected to a 31-day running average before computing values above. Cloud cover was subjected to a 5-day running average due to gaps in observations. Precipitation was not averaged. Standard deviations in columns 5 and 6 are standard deviations of the observed and the (simulated-observed) running-averaged time series, respectively.

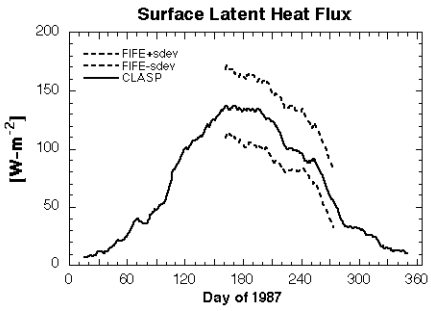

Figure 5. Time series of surface latent heat flux during 1987 from FIFE observations and CLASP. FIFE curves are each time's average over all observing instruments plus or minus the standard deviation among instruments. All curves have been subjected to a 31-day running average.

perature dependent. In the model's original G_{LEAF} formula, substantial evapotranspiration could occur in spring as temperatures warmed above freezing. Although FIFE surface evapotranspiration observations in 1987 do not begin until May 27, model behavior suggested that simulated E was too large in spring, resulting in a soil moisture deficit and weak evapotranspiration later in the summer. We delayed the onset of substantial evapotranspiration in the model by shifting the G_{LEAF} function toward higher temperatures by increasing T_{oo}. We chose the final value (Table 4) to give adequate surface latent heat flux in midsummer.

3.3.5. Canopy reservoir

[44] The canopy reservoir depth is proportional to LAI. We set the reservoir depth to (0.1 mm × LAI). The depth/LAI ratio was constrained to be between two extremes: having a relatively deep reservoir that allows too little water to reach the ground and having a canopy reservoir of negligible depth and, hence, negligible influence. For ratios of 0.1 mm/LAI and smaller, ~85% of water from modest to intense storms (precipitation >10 mm/d) fell through to the surface, consistent with results reported by *Dingman* [1994], though here the vegetation is prairie grass. Larger ratios yielded much less throughfall. The adopted ratio is also the same as used by *Bonan* [1996] in his detailed SVAT.

3.3.6. Calibrated model

[45] Comparisons of the calibrated model versus FIFE observations appear in Figures 5–11 and Table 5. Surface

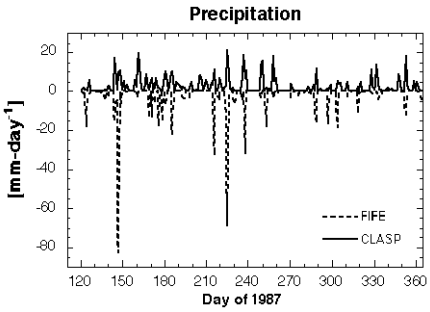

Figure 6. Time series of daily precipitation during 1987 from FIFE observations and CLASP. Observed precipitation has been multiplied by −1 to distinguish the two curves.

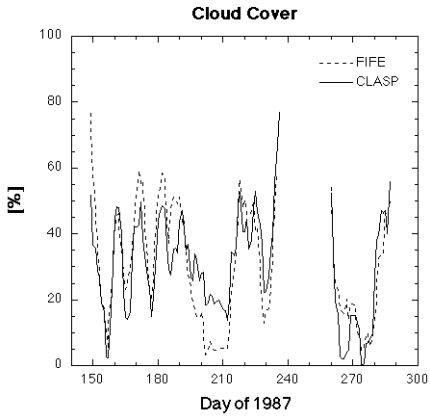

Figure 7. Time series of cloud cover during 1987 from FIFE observations and CLASP. Both curves are subjected to a 5-day running average.

latent heat flux from FIFE observations and the calibrated CLASP appear in Figure 5. The CLASP time evolution falls approximately in the middle of the two FIFE curves and thus reproduces well surface latent heat flux during the 1987 period of observations. The bias between CLASP and FIFE observations is small compared to the flux itself. Similarly, the standard deviation of the CLASP minus FIFE time series (after a 31-day running average) is small compared to the observed flux's variability, as measured by the standard deviation of the FIFE time series.

[46] Comparison of observed and simulated precipitation (Figure 6) shows that daily simulated values reproduce well the frequency of rainfall events. Although the model tends to produce more precipitation on days with greater observed precipitation, it does not reproduce the most intense daily values. This is not surprising, as the analysis providing the model's boundary conditions has a grid spacing (~165 km) that is much coarser than the ~15-km width and breadth of the FIFE observation domain. As a consequence, the external forcing of precipitation events will be spatially smoothed, and thus somewhat muted, compared to that experienced by the actual atmosphere in the FIFE domain. The smoothing will also result in days with external forcing larger than that occurring in the FIFE observing domain. The bias in time-average CLASP precipitation rate versus FIFE observations is relatively small. The temporal standard deviation of CLASP minus FIFE time series is somewhat larger (7.7 mm/d), although

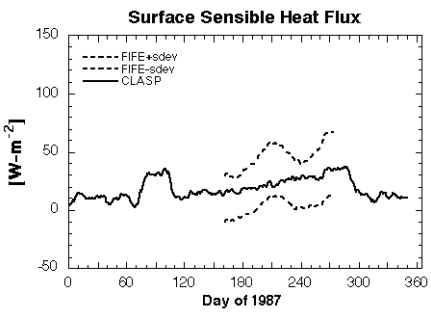

Figure 8. As Figure 5 but for surface sensible heat flux.

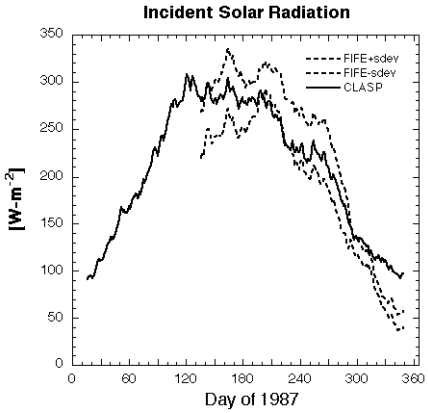

Figure 9. As Figure 5 but for incident solar radiation at the surface.

smaller than the temporal standard deviation of the daily observations (8.2 mm/d).

[47] Daily cloud cover fluctuates rapidly in the observations and the model (Figure 7), with the model generally matching the observations well over most of the period. We subjected the cloud cover time series to a 5-day running average because of a data gap from days 239 to 257 which considerably reduces the time span allowing averaging.

[48] Other simulated surface energy fluxes (sensible heat, incident solar radiation, downward infrared radiation, heat into the soil) generally compare well with observations. Surface sensible heat flux has acceptable values during the observing period (Figure 8) with small bias and small standard deviation in the CLASP minus FIFE time series (Table 5), although it does not capture a slow monthly variability seen in the observations. Incident solar radiation at the surface agrees well with FIFE observations (Figure 9) except at the end of the year, when it is larger. For both the observations and the simulation, the envelope of daily values (not shown) gradually declines toward the end of the year, and the model's envelope is nearly coincident with the observation's envelope. However, over the last 30 days of the year, the simulated daily values tend to lie closer to the envelope than the observations. This indicates that the model's cloud cover is deficient during this period. The FIFE cloud cover data set unfortunately terminates before this point, preventing a fuller comparison of cloud cover.

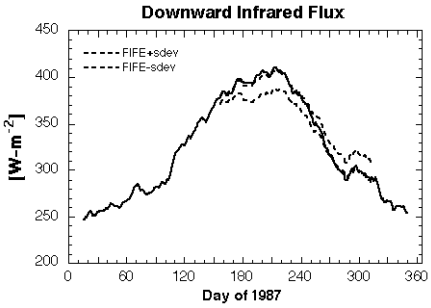

Figure 10. As Figure 5 but for downward infrared radiation at the surface.

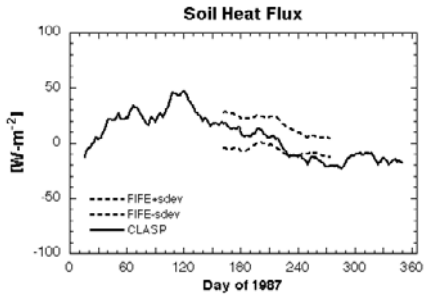

Figure 11. As Figure 5 but for heat flux at the surface into the soil. Positive flux heats the soil.

The simulated infrared radiation from the atmosphere to the surface also compares well with FIFE observations (Figure 10). During the last 30 days of the year, observations were sporadic, so this period is deleted from the comparison. Finally, the model's simulation of energy flux into the soil (Figure 11) agrees well with the FIFE observations except at the end of the observation period, when the model simulates more energy leaving the soil than given by the observations.

3.4. Validation

[49] For CLASP validation we continued the run of the fully calibrated model through the end of the NGM data set in early 1994, thus giving a total of 9 simulated years (1985–1993). FIFE data for 1988 and 1989 provide the primary observations for validating model behavior. We also use river discharge measurements for 1985–1993 and water table estimates for 1989– 1993 to complete evaluation of water flow through the fully coupled system.

[50] The next set of figures use FIFE observations for 1988 and 1989 and were constructed in the same manner as the calibration figures: FIFE observations are presented as the instrument average given by *Betts and Ball* [1998] plus or minus the standard deviation of the instrument average. In addition, Tables 6a and 6b give biases of CLASP output and standard deviations of the CLASP minus FIFE time series for periods that the field measurements are available.

[51] For surface latent heat flux (Figure 12), CLASP values are relatively low compared to FIFE observations in 1988 but are closer in 1989. *Betts and Ball* [1998] note that FIFE observations for the region's water budget do not balance. The imbalance is worse for 1988 than for 1987. In addition, even though the FIFE region experienced drought in 1988, the 1988 surface latent heat flux observations are close in magnitude to the 1987 observations. These features of the observations suggest some caution in using them to assess the model. Nonetheless, the FIFE data represent a consensus of measurements by instruments in the field, and the model is deficient versus these observations in 1988. However, any deficiency in the 1988 simulation is not permanent, as the model reproduces the 1989 conditions well.

[52] Low values of surface latent heat flux do not occur uniformly across the simulation domain (e.g., Figure 13). Note the spatial correspondence between high latent heat flux values in Figure 13 and lowlands in Figure 3. During dry periods especially, the two-way coupling of model

Table 6a. As Table 5 but for 1988 Validation Period[a]

	Comparison Period (Julian Days)	Observation Mean	CLASP-FIFE Mean	Observation Standard Deviation	CLASP-FIFE Standard Deviation
Latent heat, W m^{-2}	133–249	115	−48	18	25
Precipitation, mm d^{-1}	1–365	1.4	−0.2	5.5	5.4
Sensible heat, W m^{-2}	133–249	32	+ 33	10	23
Incident solar, W m^{-2}	146–248	266	+ 22	20	18
Downward infrared, W m^{-2}	*	336	−19	64	18
Heat flux into soil, W m^{-2}	133–249	−6.4	−0.3	3	7

[a] Because of gaps in observations, a 5-day (rather than 31 days) running average was applied to downward infrared radiation. Asterisk: = 48–55, 65–96, 136–182, 192–209, 223–363.

rivers, aquifers, and root zones supplies additional water for evapotranspiration that would otherwise flow from the domain via its river network. Low-lying areas along the domain's river network thus have larger transpiration. The transport of water from the higher elevations by rivers to low-lying aquifers and then root zones causes the domain's monthly evapotranspiration to be as much as 50% larger in late 1988 that it is in a simulation otherwise identical except that root zone encroachment by the aquifer is not allowed (not shown).

[53] Precipitation simulation for 1988 and 1989 (Figure 14) reproduces features of the 1987 FIFE-CLASP comparison: the model tends to capture the frequency of wet and dry periods well but has more difficulty matching the observed magnitude, especially for intense rain events. CLASP bias versus FIFE is acceptable in 1988 (Table 6a) but is rather large in 1989 (Table 6b). Much of the bias in 1989 is due to very intense precipitation events that the model does not capture. The model's inability to capture these events further underscores the difficulty of reproducing observed precipitation for a relatively small area compared to the resolution of the driving fields.

[54] Cloud cover observations were not available from the *Betts and Ball* [1998] data set for 1988 and 1989. Surface fluxes of incident solar radiation (Figure 15) indicate that the model produces reasonably good cloud cover with bias toward less cloud cover than actually occurred in 1988. Other energy fluxes at the surface (sensible heat flux, downward infrared radiation, heat flux into the soil) compare acceptably well (Figures 16, 17, 18), except that the CLASP sensible heat flux tends to be too large in 1988, consistent with its latent heat flux tending to be too small. As with the latent heat flux, the surface sensible heat flux returns to values similar to the FIFE observations in 1989.

[55] Overall, CLASP does a reasonably good job of simulating climatic behavior of water and energy cycles for the 2-year validation period when judged against FIFE observations. Two years after the calibration period, there do not appear to be any persistent trends in the model which cause permanent bias versus observations. Indeed, the model's surface sensible and latent heat fluxes appear to recover well in 1989 from whatever bias they had in 1988. The results do suggest, however, that the model may exaggerate extreme dry behavior.

[56] Wells located along the Kansas River (Table 7) provide estimates of water table heights for the years 1989–1993 [*Putnam et al.*, 1997]. The model has a relatively simple aquifer that does not include details of the region's geology. However, year-to-year fluctuations in observed and simulated water balances at the surface should produce fluctuations in groundwater recharge which yield water table fluctuations. Thus for the period of water table observations, we remove the 5-year average in observed and simulated water tables and compare aquifer height variability. In addition, because we are not attempting to simulate detailed hydrologic behavior within each CLASP cell, we average together the fluctuations from all 10 well sites to examine how well the model simulates the overall interannual variability of the water table along the portion of the Kansas River contained in the simulation domain.

[57] Water table measurements for the wells in Table 7 occur during January or February of each year. For comparison we extract aquifer depth on January 15 of each year for the middle node of 10 CLASP cells closest to the wells. The middle node is representative of fluctuations occurring in the other nodes of a cell. Aquifer depths change slowly enough that the model-observation comparison is insensitive to the specific date chosen for simulated output. Figure 19 shows the simulated and observed water table variability. The model's interannual variability is comparable to the observed variability. The model's water table evolution is part of a long-term decrease initiated

Table 6b. As Table 5 but for 1989 Validation Period[a]

	Comparison Period (Julian Days)	Observation Mean	CLASP-FIFE Mean	Observation Standard Deviation	CLASP-FIFE Standard Deviation
Latent heat, W m^{-2}	204–226	90	+ 6	22	23
Precipitation, mm d^{-1}	1–313	2.5	−1.0	8.0	8.0
Sensible heat, W m^{-2}	204–226	44	−13	8	22
Incident solar, W m^{-2}	204–223	267	−34	18	41
Downward infrared, W m^{-2}	16–298	336	−13	50	7
Heat flux into soil, W m^{-2}	204–226	−3	−1	5	12

[a] All fluxes except for downward infrared were subjected to just a 5-day running average due to shortness of observation record. Downward infrared radiation was subjected to a 31-day running average, and precipitation was not averaged.

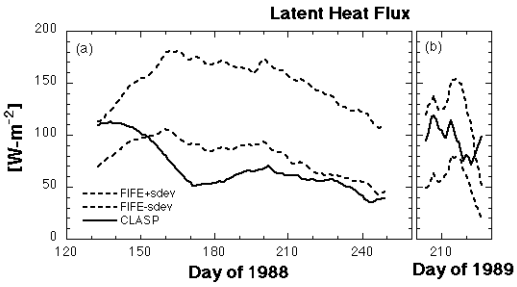

Figure 12. Time series of surface latent heat flux during (a) 1988 and (b) 1989 from FIFE observations and CLASP, for the periods when FIFE observations are available in the *Betts and Ball* [1998] archive. FIFE curves are each time's average over all observing instruments plus or minus the standard deviation among instruments. Curves for 1988 are subjected to a 31-day running average; curves for the shorter 1989 observing period are subjected to a 5-day running average.

during the 1988 drought that does not reverse until the large 1992 rainfall that contributed to flooding in this region in 1993. The observed water tables, on the other hand, do not show the simulation's downward trend for 1989–1992, suggesting that the real-world aquifers along the Kansas River recovered more rapidly from the 1988 drought than the CLASP aquifers. There is also greater spatial deviation in water table fluctuations in the observations than in the model, consistent with the relatively simple groundwater scheme used by the model. Discrepancies between observed and simulated groundwater levels are comparable with published distributed parameter surface water/groundwater models [e.g., *Konikow and Bredehoeft*, 1974].

[58] To compare simulated and observed river discharges, we searched for gauging stations with an upstream basin lying entirely within the simulation domain. The observed discharges were then compared with those generated entirely

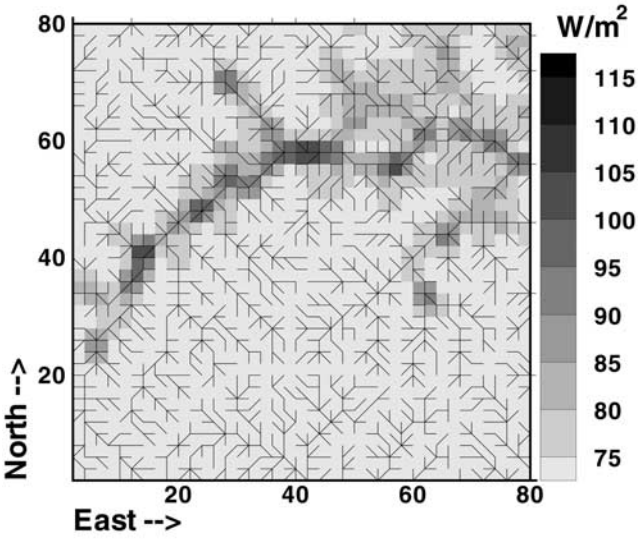

Figure 13. Simulated surface latent heat flux in each of the model's cells for July 1988.

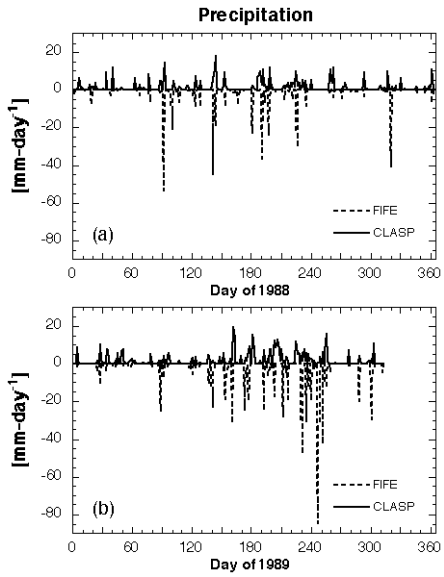

Figure 14. Time series of daily precipitation during (a) 1988 and (b) 1989 from FIFE observations and CLASP. Observed precipitation has been multiplied by −1 to distinguish the two curves.

by the model. There are three basins with gauged streams [*USGS*, 2000] located in the simulation domain (Table 8): Mill Creek, Kings Creek, and the Neosho River. The Neosho River has a dam just upstream from the gauging station used, but this control structure does not appear to obscure the basin's interannual variability in discharge production. More important, the observed discharge in each basin is about 2.5–4 times greater than the simulated discharge (Figure 20; note separate axes for observed and simulated values). This difference occurs both in 1987, when the surface water balance is calibrated, and in the overall average. Groundwater recharge for this region is a relatively small difference between much larger precipitation and evapotranspiration, so any small error in either can manifest itself as a relatively large error in long-term discharge.

[59] In Figure 20 the observed discharge shows proportionately greater temporal variability than the simulated discharge, with the ephemeral Kings Creek having substantial periods of zero discharge. The relatively simple root-zone and aquifer system of the model appears to dampen the model's response to interannual variations in precipitation

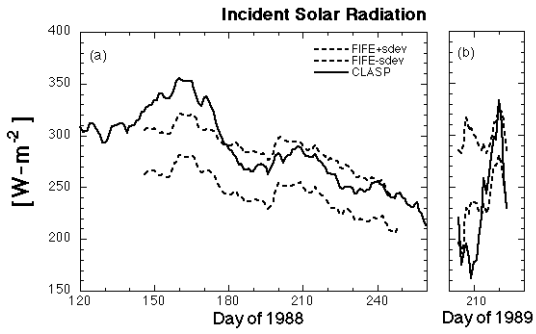

Figure 15. As Figure 12 but for incident solar radiation at the surface.

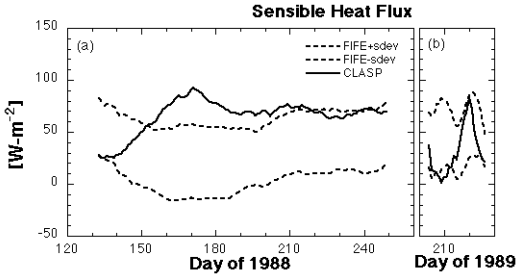

Figure 16. As Figure 12 but for surface sensible heat flux.

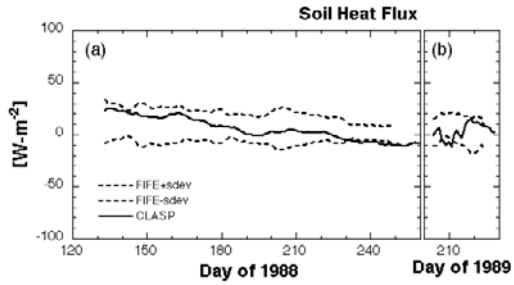

Figure 18. As Figure 12 but for heat flux at the surface into the soil. Positive flux heats the soil.

and evapotranspiration. Including a two-way interaction between root zone and aquifer increases the temporal variability of the model's discharge but not sufficiently to match observed variability.

[60] We believe that more realistic representation of precipitation's spatial distribution, overland flow processes, and perched aquifers could further improve model calibration. To test the first mechanism, we conducted a sensitivity analysis in which precipitation was spatially disaggregated. The model simulations presented above had precipitation spread uniformly across the surface, whereas actual precipitation will have spatial variability over the scales resolved by the surface cells. We performed a sensitivity analysis that spatially disaggregated precipitation in a simple way, in order to assess the potential importance of including spatial variability. In these tests, the atmosphere's precipitation during a day was assumed to fall only on N% of the cells. The cells receiving precipitation were chosen randomly, and a new set was chosen each day. Figure 21 shows the time evolution of total discharge from the model domain and aquifer water volume for the standard (uniform precipitation) case and for the cases $N = 25$ and $N = 10$. With precipitation falling more intensely on fewer cells, groundwater recharge occurs more frequently and with larger volume. Consequently, river discharge from the domain increases by 81% and aquifer water volume increases by 13% for $N = 10$. The variability of river discharge also increases markedly. In addition, for $N = 10$, the duration of time after 1988 before the aquifer starts filling again is much shorter, so aquifer depletion is less. The results suggest that implementing a precipitation disaggregation scheme within this domain of 6400 km^2 could account for much of the observation-simulation discharge differences in Figure 20.

[61] Finally, as intended, the model can close its water budget. Table 9 shows 9-year averages for each of the terms in the water budget equations. Because of the extreme drought (1988) and flood (1993) periods during the simulation, storage changes in the aquifer are significant. Atmospheric water convergence in Table 9 is diagnosed from the model's upstream method for specifying horizontal tendencies in the atmosphere. One can also compute C directly from the NGM analyses. This computation can be rather noisy due to difficulties in computing divergences in atmospheric data sets [cf. *Randall and Cripe*, 1999]. Assuming that the noisiness is random and thus small under multiyear averaging, the directly computed C for this period is 0.6 mm/d. This suggests a potential for larger groundwater recharge and discharge. E and P would only have to change by a few percent each to realize this potential.

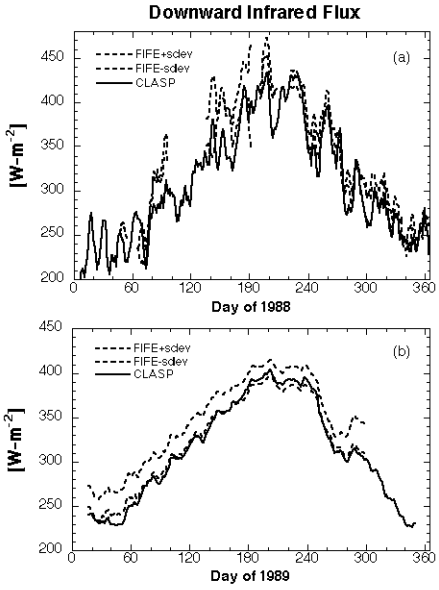

Figure 17. As Figure 12 but for downward infrared radiation at the surface. Curves for 1988 are subjected to only a 5-day running average because the observed record has several gaps.

4. Conclusion

[62] We have presented a model designed to study the coupled land-atmosphere hydrologic cycle, following water through a wide spectrum of transformations from its inflow into a region by horizontal, atmospheric transport through surface-atmosphere exchange processes and

Table 7. Well Sites

County	Well Number
Geary	11S 06E 27CBB 01
Pottawtomie	09S 11E 19CDB 01
Pottawtomie	09S 11E 31DCC 01
Pottawtomie	09S 11E 32ADC 01
Pottawtomie	10S 10E 10DBC 01
Pottawtomie	10S 11E 04DBC 01
Pottawtomie	10S 12E 07BBC 01
Riley	10S 09E 17BDD 01
Waubansee	10S 10E 15DCC 01
Waubansee	10S 12E 29ADD 01

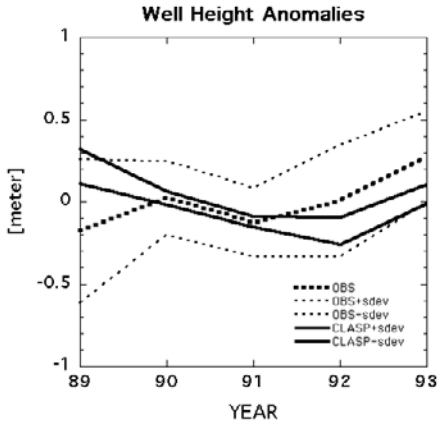

Figure 19. Deviation of water table from simulated and observed 1989–1993 averages, averaged over 10 sites. Observational curves include the 10-site average and the average plus/minus the intersite standard deviation. CLASP curves include only the corresponding 10-site average plus/minus the standard deviation among CLASP sites.

aquifer recharge to outflow as river discharge. The model is intended to help improve our capability to simulate the global-scale hydrologic cycle and to close water budgets. It therefore is designed to emulate a grid box of an atmospheric general circulation model but with land processes simulated at finer resolution. The model thus forms a test bed for developing continental-scale simulation of the land-atmosphere hydrologic cycle and allows us to address issues such as land-surface heterogeneity in multiyear simulation. Because the model aims at improving our understanding of macroscale hydrologic processes in climate simulation, its component parts in this initial formulation are relatively simple to aid interpretation of model behavior. However, it has also been designed to allow relatively straightforward implementation of alternative numerical models of component processes.

[63] We have developed CLASP following a data-rich approach that uses the wide variety of observations available from the FIFE campaign to calibrate and validate the model. The variety of observations has produced a thorough depiction of model capability and helped constrain freedom to adjust model parameters arbitrarily. The model generally captures well temporal behavior in water and energy cycles. In addition, the potentially bidirectional flow of water between model reservoirs provides additional water for evapotranspiration during dry periods by allowing river discharge generated in the model's uplands to reenter aquifers and root zones in lowlands. This behavior increases monthly average evapotranspiration for the domain as a whole by up to 50%.

[64] The model does have deficient surface latent heat flux versus observations during the drought summer of

Table 8. Discharge Stations

Basin	USGS Station Number
Kings Creek near Manhattan, Kansas	06879650
Mill Creek near Paxico, Kansas	06888500
Neosho River at Council Grove, Kansas	07179500

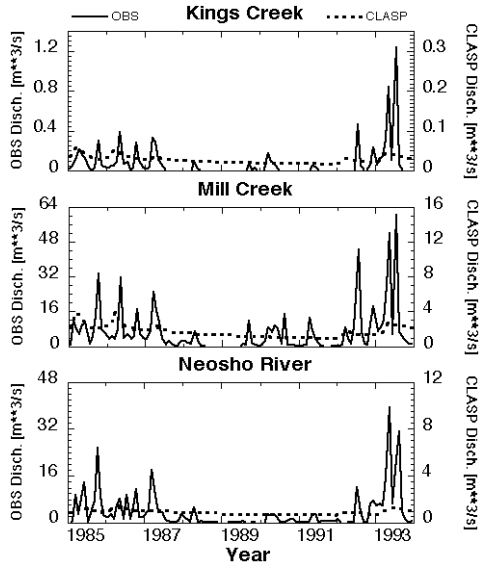

Figure 20. Observed (solid) and simulated (dotted) discharge for (a) Kings Creek, (b) Mill Creek, and (c) Neosho River. Note the separate scales for observed and simulated discharges.

1988. The results suggest that the model's root zone is overly responsive to drought conditions, though it does recover by the following summer to give surface sensible and latent heat fluxes that are similar to observations. Comparison of simulated versus observed water tables shows that the model can reproduce the observed degree of interannual variability fairly well. However, discharge in the model's river network is deficient versus observations, even in 1987, when the model was calibrated to

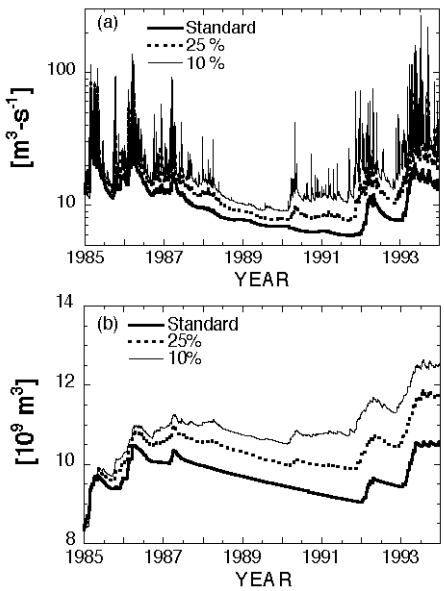

Figure 21. Simulated (a) discharge and (b) volume of aquifer water for the standard CLASP and for cases where precipitation is distributed on only 25% or 10% of the model's cells, with the set receiving precipitation changing daily.

Table 9. CLASP 9-Year Average Water Budgets[a]

Model Domain	Budget Equation	Simulated Values, mm d^{-1}
ATMOS	$\frac{dQ}{dt} = C + E - P$	0.00 = +0.26 + 1.84 − 2.10
SVAT	$\frac{dW}{dt} = P - E - R_0$	0.00 = +2.10 − 1.84 − 0.26
GW/SW	$\frac{dV_{a-r}}{dt} = R_0 - D$	+0.11 = +0.26 − 0.15

[a] Terms under simulated values are in the same order as their corresponding equations to the left.

agree with observed time average precipitation and evapotranspiration. This behavior suggests that modifications are needed in the model's treatment of runoff, since river discharge also varies relatively slowly in time versus observations. Sensitivity tests suggest that spatial disaggregation of precipitation may be an important modification to include in future versions, though further improvements in the model's overland runoff and representation of perched aquifers are probably also necessary. Enhanced overland runoff would increase model sensitivity to spatial disaggregation of precipitation.

[65] Despite the model's relatively sluggish aquifer-river responsiveness, CLASP does produce a closed water budget for its complete set of reservoirs (e.g., Table 9), allowing one to track water fully through the simulated domain. Its simulation of land surface and atmosphere hydrologic behavior appears sufficiently robust for examining multiyear feedbacks of coupled land-atmosphere interactions in the hydrologic cycle. Thus the model can be used to examine such issues as effects on the regional hydrologic cycle of vegetation distributions that are subgrid in scale relative to the width of the atmospheric column. Earlier work using the atmospheric portion of this model, for example, examined how and when subgrid distributions of sea surface temperature influences air-sea interaction [*Gutowski et al.*, 1998]. An important capability of the model in this regard is its ability to perform multiyear runs efficiently so that the model can simulate simultaneously the fast evolution of the atmospheric hydrologic cycle and the slow evolution of subterranean water. One current extension of the model taking advantage of this capability, while also including a more precise representation of spatially distributed terrestrial features, is a coupling to the U.S. Geological Survey subsurface model MODFLOW [*McDonald and Harbaugh*, 1988].

Notation

A_r = river cross-sectional area.
C horizontal convergence of atmospheric water transport.
C_{at} atmospheric conductance.
C_{can} canopy conductance.
C_{dh} surface drag coefficient for sensible heat.
C_{dm} surface drag coefficient for momentum.
C_p specific heat of air, at constant pressure.
CP convective precipitation falling outside the convective cloud.
C_s soil (root zone) heat capacity.
C_{deep} deep-soil heat capacity.
D net river discharge from model domain.
D_d downstream discharge from a river reach.
D_u upstream discharge into a river reach.
E evapotranspiration
G_{HD} conductance coefficient for absolute humidity deficit.
G_{LEAF} conductance coefficient for leaf temperature.
G_{LWP} conductance coefficient for leaf-water potential.
G_{SOL} conductance coefficient for net solar radiation.
H surface sensible heat flux.
H_{deep} deep soil heat flux.
L latent heat of vaporization
LAI leaf-area index.
$\vec{\mathrm{M}}$ surface-atmosphere momentum exchange.
P precipitation
Q atmospheric precipitate water.
$Q_{b\text{-}f}$ aquifer's base flow.
RD rooting depth
$\mathrm{RH}_{\mathrm{eff}}$ effective saturation relative humidity.
R_{hyd} hydraulic radius of river.
R_{net} net radiative flux at the surface.
R_o groundwater recharge.
R_p rainfall directly onto a river.
S slope of the river's energy grade line.
S_y specific yield
T atmospheric temperature.
T_a temperature of the lowest atmospheric layer.
T_{deep} deep-soil temperature.
T_h^f transmissivity for groundwater flow.
T_s soil-surface temperature.
T_{OO} lower limit on T_a for nonzero G_{LEAF}.
$V_{a\text{-}r}$ volume of water in combined aquifer-river network.
V_{river} volume of water in a river element.
$\vec{V}$ horizontal wind.
$\vec{V}_a$ horizontal wind in the lowest atmospheric layer.
W total soil moisture.
W_{avail} available soil moisture.
$\Delta X_{\mathrm{river}}$ length of a surface cell's river element.
$c_{\max}$ maximum leaf conductance.
c_p heat capacity of air at constant pressure.
e_a vapor pressure of the lowest atmospheric layer.
e_s saturation vapor pressure.
f Coriolis parameter, = 2 sin (latitude).
g gravitational acceleration.
h water table elevation.
h_{river} depth of river.
k von Karman constant.
n_m Manning's roughness coefficient.
p air pressure.
q atmospheric water vapor specific humidity.
t time.
u west-east component of $\vec{\mathrm{V}}$.
v south-north component of $\vec{\mathrm{V}}$.
w vertical wind.
w_{river} width of river.
x west-east coordinate.
y south-north coordinate.
z vertical coordinate.
z_a midlevel of the lowest atmospheric layer.
z_o surface roughness.
z_S surface elevation.
Ω rotation rate of the Earth.

γ psychrometric constant.
θ atmospheric petential temperature.
κ R/C_p.
ρ air density.

[66] **Acknowledgments.** This research was supported by the U.S. Department of Energy under grant DE-FG02-92ER6147. Additional computational support came from the National Science Foundation Earth Sciences Instrumentation and Facilities Program under grant EAR-94-04873. Support from the Gibson Hydrogeology Endowment and the McKnight Land Grant Professorship Program at the University of Minnesota are also gratefully acknowledged. We obtained NGM analyses from the archives of the U.S. National Center for Atmospheric Research. We thank the reviewers for their helpful comments and questions. We thank C. Winkler, C. do Espirito Santo, S. Karakoy, S. Kiehne, B. Lebeck, P. Morin, P. Nendick, and D. Slawinski for assistance with programming and graphics. We also thank J.-F. Louis, K.-N. Liou, and K. Emanuel for providing code that was adapted for constructing CLASP.

References

Betts, A. K., and J. H. Ball, FIFE surface climate and site-average data set 1987–89, *J. Atmos. Sci.*, *55*, 1091–1108, 1998.

Bonan, G. B., A land surface model (LSM version 1.0) for ecological, hydrological, and atmospheric studies: Technical description and user's guide, *NCAR Tech. Note, NCAR/TN-417+STR*, 150 pp., Natl. Cent. for Atmos. Res., Boulder, Colo., 1996.

Deardorff, J. W., Efficient prediction of ground surface temperature and moisture with inclusion of a layer of vegetation, *J. Geophys. Res.*, *83*, 1889–1903, 1978.

Dickinson, R. E., A. Henderson-Sellers, and P. J. Kennedy, Biosphere-Atmosphere Transfer Scheme (BATS) version 1e as coupled to the NCAR Community Climate Model, *NCAR Tech. Note, NCAR/TN-387+STR*, 72 pp., Natl. Cent. for Atmos. Res., Boulder, Colo., 1993.

Dingman, S. L., *Physical Hydrology*, 575 pp., Macmillan, Old Tappan, N. J., 1994.

Duan, Q. Y., J. C. Schaake, and V. I. Koren, FIFE 1987 water budget analysis, *J. Geophys. Res.*, *101*, 7197–7207, 1996.

Emanuel, K. A., A scheme for representing cumulus convection in large-scale models, *J. Atmos. Sci.*, *48*, 2313–2335, 1991.

Famiglietti, J. S., and E. F. Wood, Evapotranspiration and runoff from large land areas: Land surface hydrology for atmospheric general circulation models, in *Climate Models: Observations, Models, and Analyses*, edited by E. F. Wood, pp. 17–204, Kluwer Acad., Norwell, Mass., 1991.

Famiglietti, J. S., E. F. Wood, M. Sivapalan, and D. J. Thongs, A catchment scale water balance model for FIFE, *J. Geophys. Res.*, *97*, 18,997–19,007, 1992.

Garratt, J. R., *The Atmospheric Boundary Layer*, 316 pp., Cambridge Univ. Press, New York, 1992.

Gelhar, L. W., and J. L. Wilson, Groundwater quality modeling, *Ground Water*, *12*, 399–408, 1974.

Gutowski, W. J., Z. Ötles, and Y. Chen, Effect of ocean-surface heterogeneity on climate simulation, *Mon. Weather Rev.*, *126*, 1419–1429, 1998.

Hostetler, S. W., and F. Giorgi, Use of output from high-resolution atmospheric models in landscape-scale hydrological models, *Water Resour. Res.*, *29*, 1685–1695, 1993.

Kalnay, E., M. Kanamitsu, J. Pfaendtner, J. Sela, M. Suarez, J. Stackpole, J. Tuccillo, L. Umscheid, and D. Williamson, Rules for the interchange of physical parameterizations, *Bull. Am. Meteorol. Soc.*, *70*, 620–622, 1989.

Kanemasu, E. T., et al., Surface flux measurements in FIFE: An overview, *J. Geophys. Res.*, *97*, 18,547–18,555, 1992.

Konikow, L. F., and J. D. Bredehoeft, Modeling flow and chemical quality changes in an irrigated stream-aquifer system, *Water Resour. Res.*, *10*, 546–562, 1974.

Koster, R. D., and P. S. Eagleson, A one-dimensional interactive soil-atmosphere model for testing formulations of surface hydrology, *J. Clim.*, *6*, 593–606, 1990.

Koster, R. D., M. J. Suarez, A. Ducharne, M. Stieglitz, and P. Kumar, A catchment-based approach to modeling land surface processes in a general circulation model, 1, Model structure, *J. Geophys. Res.*, *105*, 24,809–24,822, 2000.

Levine, J. B., and G. D. Salvucci, Equilibrium analysis of groundwater-vadose zone interactions and the resulting spatial distribution of hydrologic fluxes across a Canadian prairie, *Water Resour. Res.*, *35*, 1369–1383, 1999.

Liou, K.-N., and S. C. Ou, Parameterization of infrared radiative transfer in cloudy atmospheres, *J. Atmos. Sci.*, *38*, 2707–2716, 1981.

Liou, K.-N., and S. C. Ou, Theory of equilibrium temperature in radiative-turbulent atmospheres, *J. Atmos. Sci.*, *40*, 214–229, 1983.

Liou, K.-N., and Q. Zheng, A numerical experiment on the interactions of radiation, clouds and dynamic processes in a general circulation model, *J. Atmos. Sci.*, *41*, 1513–1535, 1984.

Logaiciga, H. A., J. B. Valdes, R. Vogel, J. Garvey, and H. Schwarz, Global warming and the hydrological cycle, *J. Hydrol.*, *174*, 83–127, 1996.

Lorenz, E. N., *The Nature and Theory of the General Circulation of the Atmosphere*, 161 pp., World Meteorol. Organ., Geneva, Switzerland, 1967.

Louis, J.-F., A parametric model of vertical eddy fluxes in the atmosphere, *Boundary-Layer Meteorol.*, *17*, 187–202, 1979.

Louis, J.-F., M. Tiedtke, and J.-F. Geleyn, A short history of the operational PBL parameterization at ECMWF, in *Proceedings of the ECMWF Workshop on PBL Parameterization*, pp. 5–79, Eur. Cent. for Medium-Range Weather Forecasts, Reading, U. K., 1981.

Macpherson, G. L., Hydrogeology of thin limestones: The Konza Prairie Long-Term Ecological Research site, northeastern Kansas, *J. Hydrol.*, *186*, 191–228, 1996.

McDonald, M. G., and A. W. Harbaugh, A modular three-dimensional finite-difference groundwater flow model, in *U.S. Geological Survey Techniques of Water-Resources Investigations*, book 6, chap. A1, U.S. Geol. Surv., Washington, D. C., 1988.

Michaud, J. D., and W. J. Shuttleworth, Executive summary of the Tucson Aggregation Workshop, *J. Hydrol.*, *200*, 176–181, 1997.

National Soil Survey Center (NSSC), 2000. (Available at http://www.statlab.iastate.edu/soils/nssc/soilsdata.html)

Nie, D., T. Demetriades-Shah, and E.T. Kanemasu, Surface energy fluxes on four slope sites during FIFE 1988, *J. Geophys. Res*, *97*, 18,641–18,649, 1992a.

Nie, D., E. T. Kanemasu, L. J. Fritschen, H. L. Weaver, E. A. Smith, S. B. Verma, R. T. Field, W. P. Kustas, and J. B. Stewart, An intercomparison of surface energy flux measurement systems used during FIFE 1987, *J. Geophys. Res*, *97*, 18,715–18,724, 1992b.

Pan, Z., E. S. Takle, W. J. Gutowski, and R. W. Turner, Long simulation of regional climate as a sequence of short segments, *Mon. Weather Rev.*, *127*, 308–321, 1999.

Phillips, T. J., Documentation of the AMIP models on the World Wide Web, *PCMDI Rep. 24*, 14 pp., Lawrence Livermore Natl. Lab., Livermore, Calif., 1995. (http://www-pcmdi.llnl.gov/phillips/modldoc/amip/amip.html)

Pitman, A. J., A new parameterization of the land surface for use in general circulation models, Ph.D. thesis, 481 pp., Univ. of Liverpool, Liverpool, England, 1988.

Press, W. H., S. A. Teukolsky, W. T. Vetterling, and B. P. Flannery, *Numerical Recipes in FORTRAN, The Art of Scientific Computing*, 966 pp., Cambridge Univ. Press, New York, 1992.

Putnam, J. E., D. L. Lacock, D. R. Schneider, M. D. Carlson, and B. J. Dague, Water Resources Data—Kansas, Water Year 1996, *U.S. Geol. Surv. Water-Data Rep. KS-96-1*, 498 pp., U.S. Geol. Surv., Water Resour. Div., Lawrence, Kansas, 1997.

Randall, D. A., and D. G. Cripe, Alternative methods for specification of observed forcing in single-column models and cloud system models, *J. Geophys. Res.*, *104*, 24,527–24,545, 1999.

Roads, J. O., S.-C. Chen, A. K. Guetter, and K. P. Georgakakos, Large-scale aspects of the United States hydrologic cycle, *Bull. Am. Meteorol. Soc.*, *75*, 1589–1610, 1994.

Running, S. W., and J. C. Coughlan, A general model of forest ecosystem processes for regional applications, I, Hydrologic balance, canopy gas exchange, and primary production processes, *Ecol. Mod.*, *42*, 125–154, 1988.

Salvucci, G. D., and D. Entekhabi, Hillslope and climatic controls on hydrologic fluxes, *Wat. Resour. Res.*, *31*, 1725–1739, 1995.

Sela, J., Spectral modeling at the National Meteorological Center, *Mon. Weather Rev.*, *108*, 1279–1292, 1980.

Sellers, P. J., F. G. Hall, G. Asrar, D. E. Strebel, and R. E. Murphy, An overview of the First International Satellite Land Surface Climatology Project (ISLSCP) Field Experiment (FIFE), *J. Geophys. Res.*, *97*, 18,345–18,371, 1992.

Sellers, P. J., D. A. Randall, G. J. Collatz, J. A. Berry, C. B. Field, D. A. Dazlich, C. Zhang, G. D. Collelo, and L. Bounqua, A revised land surface parameterization (SiB2) for atmospheric GCMs, I, Model formulation, *J. Clim.*, *9*, 676–705, 1996.

Slingo, J. M., The development and verification of a cloud prediction scheme for the ECMWF model, *Q. J. R. Meteorol. Soc.*, *113*, 899–927, 1987.

Smith, E. A., et al., Area-averaged surface fluxes and their time-space variability over the FIFE experimental domain, *J. Geophys. Res.*, *97*, 18599–18622, 1992.

Smith, G. N., Geomorphology and Geomorphic History of the Konza Prairie Research Natural Area, Riley and Geary Counties, Kansas, M.Sc. thesis, 122 pp., Kansas State Univ., Manhattan, Kansas, 1990.

Stensrud, D. J., Importance of low-level jets to climate: A review, *J. Clim.*, *9*, 1698–1711, 1996.

Stewart, J. B., and S. B. Verma, Comparison of surface fluxes and conductances at two contrasting sites within the FIFE area, *J. Geophys. Res.*, *97*, 18,623–18,628, 1992.

Stieglitz, M., D. Rind, J. Famiglietti, and C. Rosenzweig, An efficient approach to modeling the topographic control of surface hydrology for regional and global climate modeling, *J. Clim.*, *10*, 118–137, 1997.

Streeter, V. L., and E. B. Wylie, *Fluid Mech*, 562 pp., McGraw-Hill, New York, 1979.

U.S. Geological Survey (USGS), Water resources of the United States, 2000. (Available at http://water.usgs.gov/)

Vörösmarty, C. J., W. J. Gutowski, M. Person, T.-C. Chen, and D. Case, Linked atmosphere-hydrology models at the macroscale, in *Macroscale Modelling of the Hydrosphere*, edited by W. B. Wilkinson, pp. 3–27, IAHS Press, Wallingford, U.K., 1993.

Vörösmarty, C. J., C. A. Federer, and A. Schloss, Potential evaporation functions compared on U.S. watersheds: Implications for global-scale water balance and terrestrial ecosystem modeling, *J. Hydrol.*, *207*, 147–169, 1998.

Walko, R. L., et al., Coupled atmosphere-biophysics-hydrology models for environmental modeling, *J. Appl. Meteorol.*, *39*, 931–944, 2000.

Wetzel, P. J., and J.-T. Chang, Evapotranspiration from nonuniform surfaces: A first approach for short-term numerical weather prediction, *Mon. Weather Rev.*, *116*, 600–621, 1988.

Winter, T., The concept of hydrologic landscapes, *Wat. Resour. Res.*, *37*, 335–349, 2001.

B. Fekete and C. J. Vörösmarty, Water Systems Analysis Group, Institute for the Study of Earth, Oceans, and Space, and Department of Earth Sciences, University of New Hampshire, Durham, NH 03824, USA.

W. J. Gutowski Jr., Department of Geological and Atmospheric Sciences, and Department of Agronomy, Iowa State University, Ames, Iowa 50011, USA. (gutowski@iastate.edu)

Z. Ötles, Frontier Science and Technology Research Foundation, Inc., 505 South Rosa Road, Suite 116, Madison, WI 53719, USA.

M. Person, Department of Geosciences, Indiana University, Bloomington, IN 47405, USA.

J. York, Department of Geology and Geophysics, University of Minnesota, Minneapolis, MN 55455, USA.